ACS APPLIED MATERIALS & INTERFACES

Research Article

www.acsami.org

Multifunctional $AlPO_4$ Coating for Improving Electrochemical Properties of Low-Cost $Li[Li_{0.2}Fe_{0.1}Ni_{0.15}Mn_{0.55}]O_2$ Cathode Materials for Lithium-Ion Batteries

Feng Wu,[†,‡] Xiaoxiao Zhang,[†] Taolin Zhao,[†] Li Li,*[,†,‡] Man Xie,[†] and Renjie Chen*[,†,‡]

[†]Beijing Key Laboratory of Environmental Science and Engineering, School of Chemical Engineering and the Environment, Beijing Institute of Technology, Beijing 100081, China

[‡]National Development Center for High Technology Green Materials, Beijing 100081, China

ABSTRACT: Layered Li-rich, Fe- and Mn-based cathode material, $Li[Li_{0.2}Fe_{0.1}Ni_{0.15}Mn_{0.55}]O_2$, has been successfully synthesized by a coprecipitation method and further modified with different coating amounts of $AlPO_4$ (3, 5, and 7 wt %). The effects of $AlPO_4$ coating on the structure, morphology and electrochemical properties of these materials are investigated systematically. XRD results show that the pristine sample is obtained with typical Li-rich layered structure and trace amount of Li_3PO_4 phase are observed for the coated samples. The morphology observations reveal that all the samples show spherical particles (3−4 μm in diameter) with hierarchical structure, composed of nanoplates and nanoparticles. XPS analysis confirms the existence of $AlPO_4$ and Li_3PO_4 phases at the surface. The electrochemical performance results indicate that the sample coated with 5 wt % $AlPO_4$ exhibits the highest reversible capacity (220.4 mA h g^{-1} after 50 cycles at 0.1*C*), best cycling performance (capacity retention of 74.4% after 50 cycles at 0.1*C*) and rate capability (175.3 mA h g^{-1} at 1C, and 120.2 mA h g^{-1} at 10*C* after 100 cycles) among all the samples. Cycle voltammograms show good reversibility of the coated samples. EIS analysis reveals that charge transfer resistance after coating is much lower than that of the pristine sample. The excellent electrochemical performances can be attributed to the effects of multifunctional $AlPO_4$ coating layer, including the suppression of surface side reaction and oxygen vacancies diffusion, the acceleration of lithium ions transport as well as the lower electrochemical resistance. Our research provides a new insight of surface modification on low-cost Li-rich material to achieve high energy as the next-generation cathode of lithium-ion batteries.

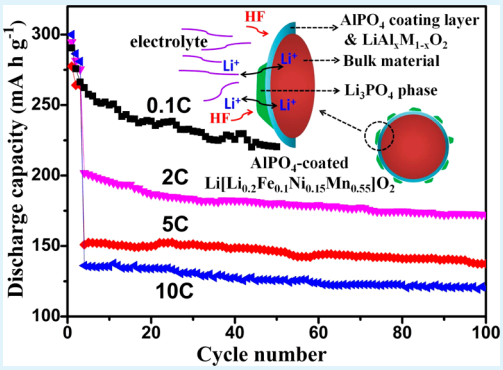

KEYWORDS: *lithium-ion battery, lithium-rich cathode, iron−manganese oxide, $AlPO_4$ coating*

1. INTRODUCTION

As the most attractive and promising candidates for electrical energy storage devices, lithium-ion batteries (LIBs) are currently being developed to provide power for our daily life from small portable electrical appliances to large electric vehicles.[1−6] Prior to other performance demand of LIBs, high capacity and low cost become the main development trends. Moreover, cost is probably the most important and fundamental issue for a broad market penetration.[5,6] The conventional cathode material like $LiCoO_2$ is limited by its theoretical capacity and high cost and cannot meet the requirements in many application fields. So it is necessary to design new materials to combine high capacity and low cost.

To meet the high capacity demand, Li-rich Mn-based cathode materials with a capacity as high as ∼250 mA h g^{-1}, first introduced by M. M. Thackeray et al., have been widely investigated in recent years, especially with the elements composition of $Li_{1.2}Mn_{0.6}Ni_{0.2}O_2$ and $Li_{1.2}Ni_{0.13}Co_{0.13}Mn_{0.54}O_2$.[7−9] On the other hand, the cost problem mostly relies on cathode materials, occupying 35% of the total cost of cells.[10] Consequently, developing cathode materials using earth-abundant elements is more desirable, and cobalt-free, Fe- and Mn-based cathodes are the most attractive choice.[11−13] Tabuchi et al. have focused on the development of $Li_{1+x}(Fe_yMn_{1-y})_{1-x}O_2$ (Fe-substituted Li_2MnO_3) cathode lying on $LiFeO_2{\cdot}Li_2MnO_3$ solid solution.[14−18] In spite of their apparently good structural properties, these cathodes exhibited poor cycle performance and rate capability. Among the strategies to improve the electrochemical performances, coating is the most simple and low-cost method used worldwide. Different types of oxides, fluorides, and phosphates are explored as the coating materials.[19−22] To realize the design concept of combination of high capacity with Fe- and Mn-based low-cost elements, the drawbacks of these materials should be addressed as well. Recently, Cho et al. reported that surface modification with $AlPO_4$ can both improve the cycling and thermal issues of cathode materials.[23−26] The mechanism of improved performances with $AlPO_4$ coating comes from the high electronegativity

Received: December 5, 2014
Accepted: January 28, 2015
Published: January 28, 2015

DOI: 10.1021/am508579r
ACS Appl. Mater. Interfaces 2015, 7, 3773−3781

Scheme 1. Schematic Diagram for the Synthetic Process of the Multifunctional $AlPO_4$ Coating

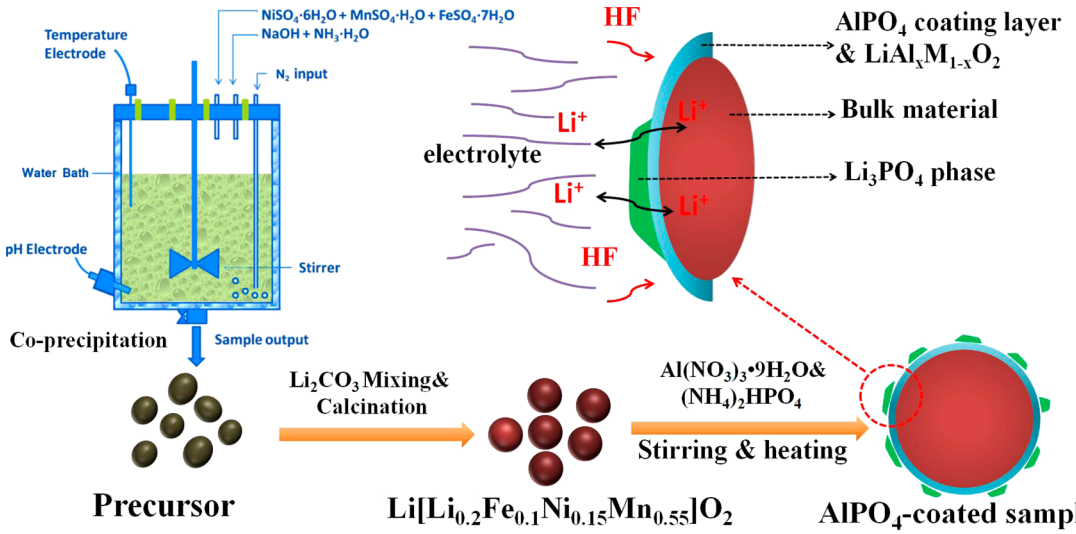

of $(PO_4)^{3-}$ polyanions with Al cation leading to strong resistance to the reaction with the electrolyte, and oxides with $(PO_4)^{3-}$ bonding have been reported to be thermally stable.[25,27] Moreover, the reduction of cathode surface exposed to the electrolyte plays an important role in metal dissolution and reducing oxygen generation.[24,26,28−30] The application of $AlPO_4$ coating on different kinds of cathode materials ($LiCoO_2$, $LiNi_{0.8}Co_{0.1}Mn_{0.1}O_2$, $LiNi_{0.8}Co_{0.15}Al_{0.05}O_2$, LiV_3O_8, $LiMn_2O_4$, et al.) have proved its positive effects on the performances.[25,30−35] But there are rare reports of coating $AlPO_4$ on the Li-rich Fe- and Mn-based cathode materials.

In this work, Li-rich Fe and Mn-based cathode materials with the elements composition of $Li[Li_{0.2}Fe_{0.1}Ni_{0.15}Mn_{0.55}]O_2$ was successfully synthesized using coprecipitation method. $AlPO_4$ coating was explored to improve the electrochemical performances of the material, and different coating amounts (3, 5, and 7 wt %) were investigated to obtain the optimal performance. The mechanism of $AlPO_4$ coating was also preliminarily discussed.

2. EXPERIMENTAL SECTION

2.1. Materials Synthesis. In this work, all the chemicals were of analytical grade and used as-received without further purification. The pristine cathode material $Li[Li_{0.2}Fe_{0.1}Ni_{0.15}Mn_{0.55}]O_2$ was synthesized by a coprecipitation method. Nickel sulfate hexahydrate ($NiSO_4·6H_2O$), manganese sulfate monohydrate ($MnSO_4·H_2O$), iron sulfate heptahydrate ($FeSO_4·7H_2O$), sodium hydroxide (NaOH), and ammonium hydroxide ($NH_3·H_2O$) were used as starting reagents to prepare the precursor particles in a continuously stirred tank reactor (CSTR). During the reaction, 2 M transition metal solution (Fe:Ni:Mn = 0.1:0.15:0.55) was slowly pumped into the reactor. The pH level was kept at 11 by controlling the added amount of the mixture solution of 4 M NaOH and 0.4 M $NH_3·H_2O$. The solution was strongly stirred at a speed of 1000 rpm. The reaction was conducted at 60 °C under an inert atmosphere by bubbling N_2 into the CSTR to mitigate the oxidation of Mn^{2+}, Ni^{2+}, and Fe^{2+}. The spherical precursor was filtered, washed with deionized water, and dried at 100 °C for 48 h. The dried precursor was well-mixed with Li_2CO_3 and then calcined at 800 °C for 15 h to obtain the pristine cathode material $Li[Li_{0.2}Fe_{0.1}Ni_{0.15}Mn_{0.55}]O_2$.

The $AlPO_4$ coating layer was performed as follows: Certain amounts of $Al(NO_3)_3·9H_2O$ and $(NH_4)_2HPO_4$ were dissolved in deionized water together until a white suspension is obtained. A desired amount of pristine powder was slowly dispersed into the suspension. Then, the resulting mixture was heated to 80 °C and stirred vigorously until the solution was evaporated to dryness. Finally, the obtained powder was calcined at 400 °C in a muffle furnace for 5 h in air atmosphere and then cooled to room temperature to get the $AlPO_4$ coated $Li[Li_{0.2}Fe_{0.1}Ni_{0.15}Mn_{0.55}]O_2$ material. The schematic diagram for the synthetic process is shown in Scheme 1. The samples with different $AlPO_4$ coating amounts of 3, 5, and 7 wt % are labeled as AC-3, AC-5, and AC-7, respectively.

2.2. Materials Characterizations. The crystalline structures of all the samples were characterized using X-ray diffraction (XRD; Rigaku Ultima IV-185) with a Cu Kα radiation source. The source tension and current are 40 kV and 40 mA, respectively. Data were acquired with a speed of 8° min^{-1} over a 2θ range of 10−80°. Morphological studies on the samples were performed using a field emission scanning electron microscope (SEM, FEI, Quanata 200f) with an accelerating voltage of 20 kV and transmission electron microscopy (TEM, JEM-2100f). Element mappings of the samples were carried out with an energy-dispersive X-ray detector (EDX) equipped on the scanning electron microscope above. The XPS measurement was performed on a PHI QUANTERA-II SXM system (Japan/Uivac-PHI, Inc.), using a monochromatized Al Kα radiation source, and the spectra were analyzed by XPSPEAK software.

2.3. Electrochemical Measurements. The working electrode for electrochemical measurements was prepared by dispersing the as-synthesized active material, acetylene black and polyvinylidene fluoride (PVDF) at a weight percent ratio of 8:1:1 in the solvent of *N*-methyl-2-pyrrolidone (NMP). Then the slurry was cast on an aluminum foil and dried overnight in a vacuum oven at 80 °C. The electrode was further roll-pressed in order to promote adhesion to the current collector. Electrochemical measurements were performed using galvanostatic cycling with coin-cells (type CR 2025). Cell assembly was carried out in an Ar-filled glovebox with oxygen and water contents less than 1 ppm, using the prepared electrode, metallic lithium foil as the counter electrode, 1 M $LiPF_6$ dissolved in ethyl carbonate (EC) and dimethyl carbonate (DMC) (1:1 by volume) as the electrolyte, and a Celgard 2400 membrane as the separator. Galvanostatic charge−discharge tests were all performed under constant current conditions using Land battery testers (Land CT2001A, Wuhan, China). The assembled cells were measured for 50 cycles at a current density of 0.1*C* and 0.2*C* (1*C* = 200 mA g^{-1}) to analyze the cycling performances of the materials. Various rates (1*C*, 2*C*, 5*C*, and 10*C*) were tested to investigate the rate capabilities of the prepared materials. It should be pointed out that a two-step charge process is employed. That is, the constant current charge step is followed by an additional constant voltage charge step until the current drops to half of its initial value.

DOI: 10.1021/am508579r
ACS Appl. Mater. Interfaces 2015, 7, 3773−3781

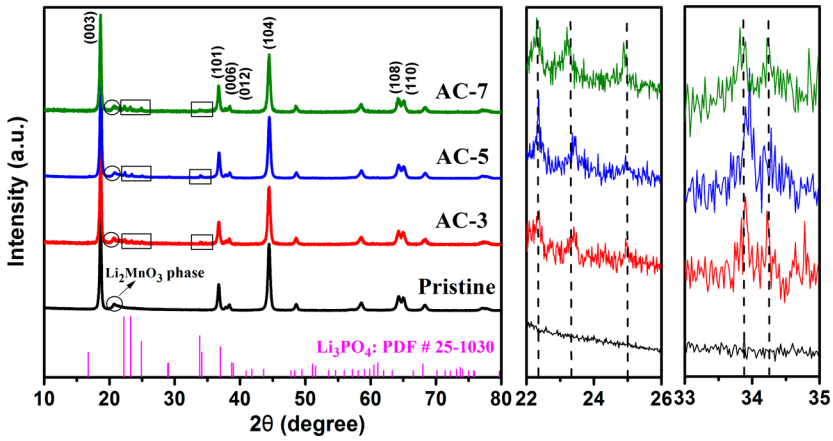

Figure 1. XRD patterns of all the samples and local magnifications of 22−26° and 33−35°.

Cyclic voltammetry (CV, 2−5 V, 0.1 mV s^{-1}) measurements were performed on a CHI660C electrochemical workstation. Electrochemical impedance spectroscopy (EIS) analysis was carried out from 1×10^5 Hz to 0.01 Hz using an IM6 electrochemical impedance analyzer with an AC perturbation signal of 5 mV. The potentials throughout the paper are referenced to the Li/Li^+ couple.

3. RESULTS AND DISCUSSION

3.1. Structural Characterizations. XRD was performed to investigate the phase structures of the as-prepared samples with different $AlPO_4$ coating amounts, as shown in Figure 1. All the XRD patterns of the samples can be indexed to the layered rock-salt form with hexagonal α-$NaFeO_2$-type structure with a space group of $R\bar{3}m$. A low-intensity peak near 2θ = 21−23° (denoted with the dotted circle) for each pattern arises from superlattice ordering of Li and Mn in the transition-metal layer, which is the characteristic of Li-rich Mn-based material close to the Li_2MnO_3 composition with $C/2m$ space group.[8,9] The clear splitting of (006)/(102) and (018)/(110) peaks demonstrates its high degree of crystallization. No distinct extra reflection peaks corresponding to any impurity phases are observed in the pristine sample. However, in the coated samples, some minor peaks originating from Li_3PO_4 phase (pointed out by square box and enlarged in the right region) emerge and become strong with the increasing coating amounts. Even with the least coating amount (3 wt %), Li_3PO_4 phase still exists obviously in the AC-3 sample. These results are consistent with previous studies, which have demonstrated the existence of Li_3PO_4 in $AlPO_4$-coated materials,[28−30] whereas the $AlPO_4$ phase is not observed because of its amorphous state. The lattice parameters of all the samples are calculated and listed in Table 1. It can be seen that parameters "a" and "c" show some variations after coating, especially for the AC-7 sample. This finding can be attributed to the partial inward diffusion of Al^{3+} from $AlPO_4$ into the surface layered lattice and the partial outward diffusion of Li^+ from the layered lattice to form Li_3PO_4 phase. High ratio of c/a usually stands for good layered structure and in this case, AC-7 sample has a higher ratio of c/a, which is speculated to come from the inward diffusion of more Al into the bulk to form solid solution with better layered structure. However, when the coating amount increases to 7 wt %, the thickest coating layer of $AlPO_4$ in AC-7 will hinder the Li^+ diffusion and sacrifice more capacity. Furthermore, the ratio of $I_{(003)}/I_{(104)}$ increases largely after coating with $AlPO_4$, indicating the decrease in Li^+/Ni^{2+} cation mixing degree in the coated samples, which is favorable to improve the crystalline nature and electrochemical performances.

Table 1. Comparison of Lattice Parameters for All the Samples

sample	a	c	c/a	$I_{(003)}/I_{(104)}$
pristine	2.8668	14.2648	4.9759	1.50
AC-3	2.8682	14.2638	4.9731	1.83
AC-5	2.8646	14.2544	4.9761	1.83
AC-7	2.8661	14.2810	4.9827	1.68

3.2. Morphologies and EDX Spectra of the Samples. Scanning electron microscopy (SEM) images of all the samples are shown in Figure 2. It can be seen that all the samples have a similar morphology, indicating that the morphology does not change after coating. The hierarchical spherical particles with 3−4 μm in diameter are composed of uniform nanoplates and nanoparticles, which are expected to increase the contact with electrolyte and therefore improve the electrochemical performances.

EDX spectroscopy was employed to investigate the composition and distribution of different elements in the samples, and the AC-5 sample is chosen to present the results. It can be seen that the sample is composed of expected elements (Fe, Ni, Mn, O, Al, and P) and the experimental contents are almost the same as that in the theoretical composition, as listed in the table inside the figure, indicating that the sample was synthesized with good stoichiometry. In addition, all the elements disperse uniformly from the mapping distribution results.

To further observe the coating layer in detail, we conducted TEM analysis of the pristine and AC-5 samples and the results are shown in Figure 3. The images clearly show the bulk nanoparticles of the pristine sample and the coating layer of the AC-5 sample in Figure 3a, c, respectively. In the HRTEM image of pristine sample, the distance of the lattice fringes was measured to be 4.8 Å, which is the typical value of layered (003) fringes of $R\bar{3}m$. The SAED image inside Figure 3b also confirms the layered structure of the pristine sample. The HRTEM image of the AC-5 sample in Figure 3d reveals a coating layer of ∼8 nm width in the amorphous phase. Also, it can be seen that the coating layer is uniformly coated on the surface of the bulk material.

3.3. XPS Analysis. The pristine and AC-5 samples were investigated by XPS to determine the surface chemical

DOI: 10.1021/am508579r
ACS Appl. Mater. Interfaces 2015, 7, 3773−3781

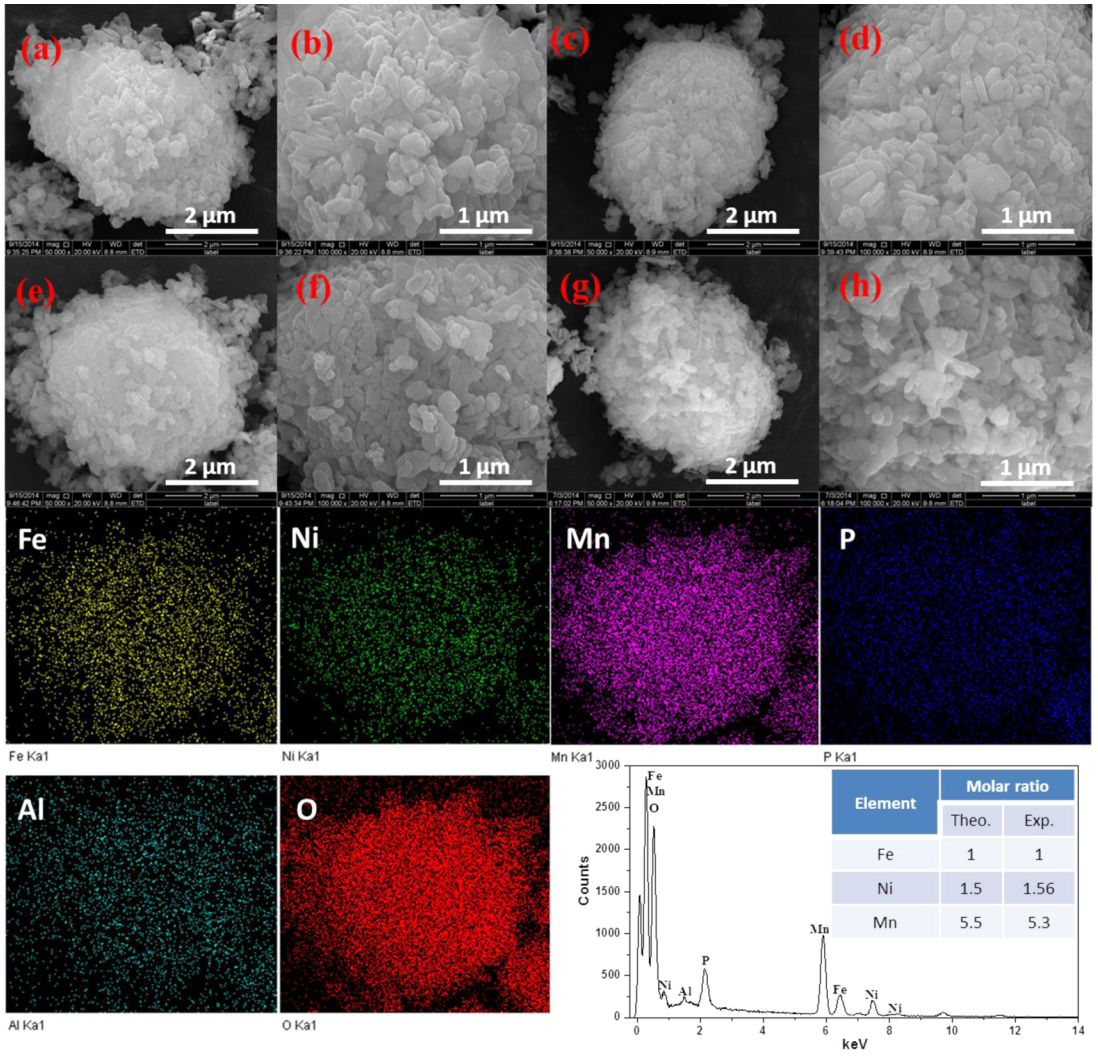

Figure 2. SEM images of all the samples: (a, b) the pristine sample, (c, d) AC-3, (e, f) AC-5, and (g, h) AC-7; EDX spectra of AC-5; inset table shows the molar ratios of the Fe, Ni, and Mn elements.

compositions and oxidation state of elements, and the results are shown in Figure 4. As expected, the Al 2p and P 2p photoemission peaks in Figure 4b, c are found for the AC-5 sample but not for the pristine sample. The binding energy (BE) of Al 2p is 74.05 eV, which is in the middle of the reported value of 74.5 eV in $AlPO_4$ bulk material and $LiAl_xM_{1-x}O_2$ (M = Ni, Co, et al.) like material.[28,29,36] This may be due to the diffusion of Al after calcination and then the formation of a solid solution at the interface between the coating and the bulk material, as discussed in the previous XRD analysis. The P 2p spectra for the AC-5 sample are assigned into two components at 134.1 and 132.2 eV, which are in good agreement with the reported values of $AlPO_4$ and Li_3PO_4, respectively.[28,29] The comparative studies of Al 2p and P 2p spectra confirm the existence of $AlPO_4$ and Li_3PO_4 phases at the surface.

The Mn $2p_{3/2}$ spectra of the two samples fit to a single peak with a BE of 642.6 eV. This value matches well with the BE reported for Mn^{4+} in literature.[11,37] The Ni $2p_{3/2}$ spectra of the samples center at 854.8 eV, which agrees with that of Ni^{2+} in NiO.[38] The Fe $2p_{3/2}$ and Fe $2p_{1/2}$ spectra exhibit two main peaks with BE of 711.3 and 725.07 eV, respectively, which should be attributed to Fe^{3+}.[12,39] Therefore, the XPS spectra show that the oxidation state of Mn, Ni, and Fe in the samples is +4, +2, and +3, respectively.

3.4. Cycling Performances. Figure 5 compares the cycling performances of the samples before and after surface modification with various $AlPO_4$ amounts at low rates of 0.1C and 0.2C. It can be seen that the discharge capacities of all the samples gradually reduce to a constant. The AC-5 sample delivers the highest initial discharge capacity of 296.4 mA h g^{-1} and maintains 220.4 mA h g^{-1} after 50 cycles at 0.1C with capacity retention of 74.4%. By comparison, the pristine sample only obtains 165.8 mA h g^{-1} after 50 cycles, which is attributed to the complete exposure to the electrolyte and unexpected surface side reactions. The existence of Li_3PO_4 phase in the material will consume some Li and (PO_4) and thus decrease discharge capacity. However, because of the low coating amount, the partially formed Li_3PO_4 phase is much less. Although the loss of some Li will consume some capacity, the inspired discharge capacity because of the coating layer is more than the decreased capacity. Consequently, the electrochemical data of coated sample show an increased discharge capacity compared to the pristine sample. The AC-7 sample with an increased coating amount of 7 wt % presents the worst cycling performance, possibly because of the excess sacrifice of capacity

DOI: 10.1021/am508579r
ACS Appl. Mater. Interfaces 2015, 7, 3773−3781

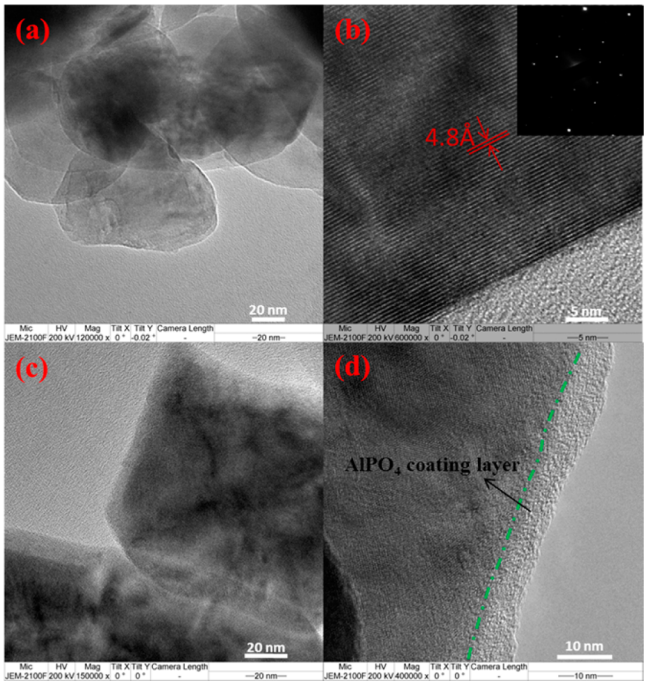

Figure 3. (a) TEM image of the pristine sample; (b) HRTEM image of Figure 3a and the corresponding SAED pattern (inset); (c) TEM image of AC-5; (d) HRTEM image of c.

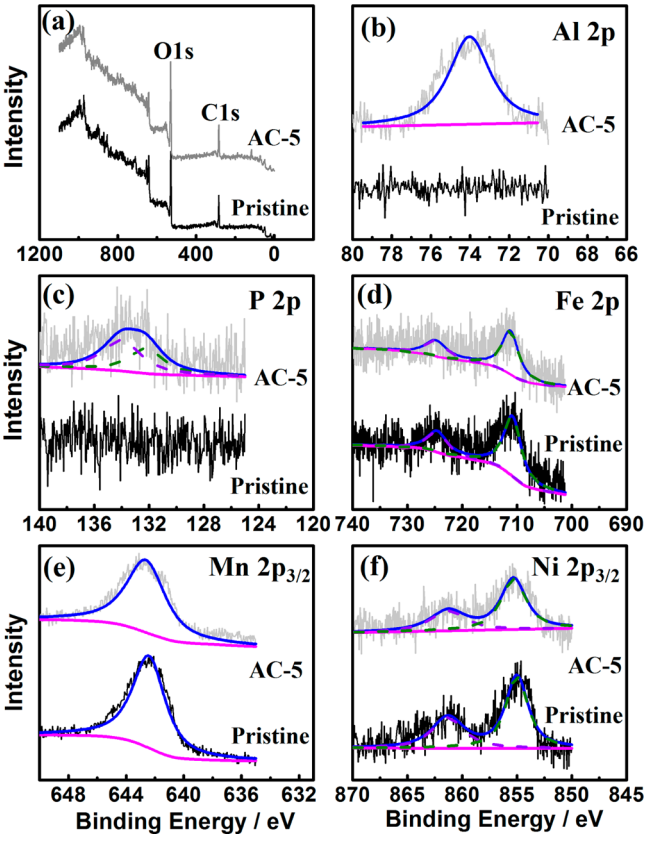

Figure 4. XPS spectra of the pristine sample and AC-5: (a) the sum, (b) Al 2p, (c) P 2p, (d) Fe 2p, (e) Mn 2p, and (f) Ni 2p core level.

from the inactive $AlPO_4$ coating layer. Similar trends can also be observed as the rate increases to 0.2*C*. So appropriate coating amount is of great importance and the 5 wt % coating

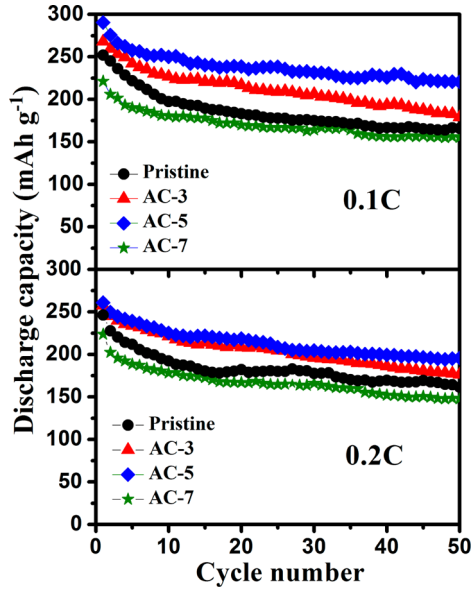

Figure 5. Cycling performances of all the samples at 0.1*C* and 0.2*C*.

amount is optimal under this circumstance. The best cycling performance of the AC-5 sample comes from the high electronegativity of $(PO_4)^{3-}$ polyanions with Al, leading to strong resistance to the reaction with the electrolyte and thus enhancing the cycling performances.[25] Moreover, it has been reported that surface modification by $AlPO_4$ can retain more oxygen ions vacancies, and then a higher discharge capacity can be obtained.[30]

3.5. Charge and Discharge Properties. The charge/discharge curves at different cycles of all the samples at 0.2*C* are shown in Figure 6, and the detailed values of electrochemical performances are summarized in Table 2. In the first charge profile, all the samples exhibit similar curve shapes of a slope below 4.5 V and plateau above 4.5 V, which is the characteristic

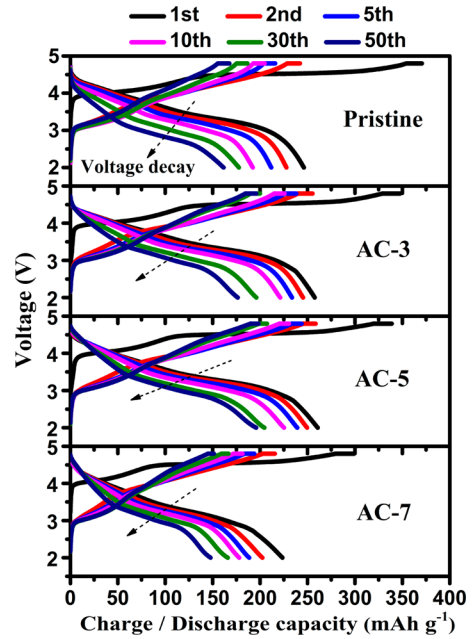

Figure 6. Charge/discharge curves of all the samples at different cycles at 0.2*C*.

DOI: 10.1021/am508579r
ACS Appl. Mater. Interfaces 2015, 7, 3773−3781

Table 2. Electrochemical Data of All the Samples at 0.2*C*

sample	initial charge capacity (mA h g^{-1})	initial discharge capacity (mAh g^{-1})	irreversible capacity (mA h g^{-1})	initial Coulombic efficiency (%)	discharge capacity after 50 cycles (mAh g^{-1})
pristine	370.5	246.2	124.3	66.5	161.5
AC-3	347.6	257.6	90	74.1	176.4
AC-5	338.8	267.2	71.6	78.9	196
AC-7	300.1	223.6	76.5	74.5	147.8

of Li-rich cathode materials.[8,9] During discharging, all the samples show almost the same trend with a long slope plateau. The pristine sample without $AlPO_4$ coating has the highest initial charge capacity of 370.5 mA h g^{-1} at 0.2C, but suffers a large irreversible capacity of 124.3 mA h g^{-1}. After coating by appropriate amount of 5 wt % $AlPO_4$, the AC-5 sample delivers higher initial discharge capacity and Coulombic efficiency of 267.2 mA h g^{-1} and 78.9%, respectively. As the coating amount increases to 7 wt %, the initial discharge capacity decreases to 223.6 mA h g^{-1}, because of the excess capacity sacrifice from $AlPO_4$ coating layer.

To further investigate the electrochemical reactions during charge/discharge processes, the corresponding differential capacity versus voltage (dQ/dV) plots of all the samples at 0.2*C* are illustrated in Figure 7. During the first charge process,

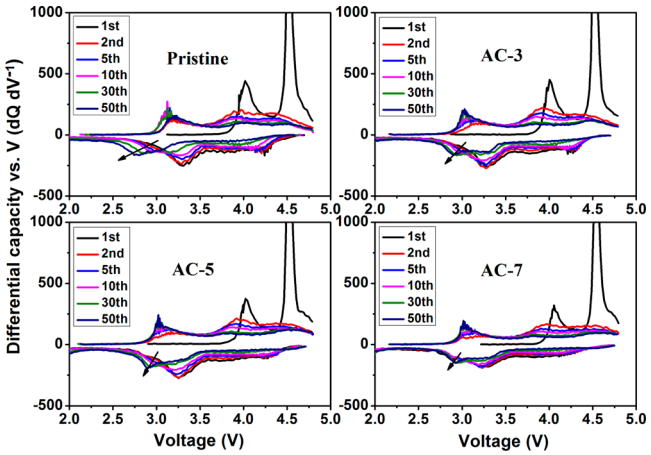

Figure 7. Corresponding charge/discharge cycle differential capacity versus voltage plots of all the samples at 0.2*C*.

the peaks at about 4.1 V have been attributed to the oxidations of Ni^{2+} to Ni^{4+} and Fe^{3+} to Fe^{4+}, and those above 4.5 V are corresponding to the Li_2O extraction from Li_2MnO_3 component.[11,17,18] For the first discharge process, no reduction peak above 4.5 V is observed because of the irreversible activation of Li_2MnO_3 in the first charge process. The peaks at about 4 V are attributed to the reductions of Ni^{4+} to Ni^{2+} and Fe^{4+} to Fe^{3+}, and the peaks at 3.3 V come from the Li-intercalation to MnO_2 component formed in the first charge process. After extended cycling, the peaks at 4 V gradually diminish and the formation of new emerging peaks at 2.8 V demonstrates the structure transformation from layered to spinel, corresponding to the reduction of Mn^{4+} to Mn^{3+}. It should be noted that the voltage decay problem of Li-rich cathode materials still exists in these samples, whereas it is clear to see that the surface modification with $AlPO_4$ can effectively delay the voltage decay, as shown in Figures 6 and 7. The reason for this is still not clear, and probably because of the role of surface coating in stabilizing the structures of interfaces.[40]

3.6. Rate Capability. Figure 8a compares the cycling performances of all the samples at various C rates (1*C*, 2*C*, 5*C*, and 10*C*) to evaluate their rate capabilities. The cells were initially cycled for 3 cycles at 0.1*C* to activate the Li_2MnO_3 component, and then charged/discharged at high rates. The discharge profiles of fourth cycle at various high rates are shown in Figure 8b. In general, the initial discharge capacities of all the samples decrease with increased rates. Among all the samples, the AC-5 sample has the highest discharge capacities at fourth cycle at various rates (210.5 mA h g^{-1} at 1*C*, 201.8 mA h g^{-1} at 2*C*, 150.9 mA h g^{-1} at 5*C*, 136.1 mA h g^{-1} at 10*C*), whereas the pristine sample delivers much less discharge capacities at all rates (171.7 mA h g^{-1} at 1*C*, 150 mA h g^{-1} at 2*C*, 97 mA h g^{-1} at 5*C*, 55.5 mA h g^{-1} at 10*C*). After 100 cycles, discharge capacities of 175.3 mA h g^{-1} at 1*C*, 172.2 mA h g^{-1} at 2*C*, 137.4 mA h g^{-1} at 5*C*, and 120.2 mA h g^{-1} at 10*C* can still be obtained by the AC-5 sample. In the discharge profiles at various high rates in Figure 8b, it can be seen that the AC-5 sample shows the most apparent discharge plateaus, whereas the pristine sample presents a declined slope, indicating the best structure stability of the AC-5 sample. The enhanced rate capability is mainly attributed to the protective coating layer and the formed Li_3PO_4 phase at the surface, which is known as a fast Li-ion conductor.[29,41]

3.7. Cyclic Voltammetry. Cyclic voltammograms of all the samples have been recorded for three cycles, as illustrated in Figure 9. In the initial cycle, the first anodic peak at approximate 4.0 V is predominantly associated with oxidation of Ni^{2+} to Ni^{4+} and Fe^{3+} to Fe^{4+},[14−18] and the second peak at a higher potential of 4.6 V is due to the irreversible electrochemical activation reaction of Li_2O extraction from the Li_2MnO_3 component. In the reverse scan, the cathodic peaks above 3.55 V are attributed to the reduction of Ni^{4+} to Ni^{2+} and Fe^{4+} to Fe^{3+}, and the ones below 3.5 V result from the reduction of Mn^{4+} (in layered MnO_2 derived from Li_2MnO_3 component) to Mn^{3+}. The results of ^{57}Fe Mossbauer spectra studied by Tabuchi et al. indicated that $Fe^{3+/4+}$ redox couple was involved in the initial charge and discharge process and no $Fe^{2+/3+}$ redox couple was found between 2.5 and 4.3 V in the Li-rich Fe-based cathode material.[14−18] The almost overlay of the second and third cycle profiles of the AC-5 sample indicates the best reversibility, which is consistent with the above electrochemical performances analysis.

3.8. Electrochemical Impedance Analysis. To better understand the improvement of rate capability, we conducted EIS of the pristine and AC-5 samples at open circuit voltage before cycling and after 100 cycles at 5*C*. The Nyquist plots of the samples and the fitted equivalent circuits are shown in Figure 10. In general, at open circuit voltage, the semicircle in the high-frequency section relates to the charge transfer resistance (R_{ct}), and the rising line in the low-frequency section is attributed to Warburg impedance (W, diffusion of Li^+ in the electrode). The intercept of the semicircle at the highest frequency with the real axis (Z') refers to uncompensated

DOI: 10.1021/am508579r
ACS Appl. Mater. Interfaces 2015, 7, 3773−3781

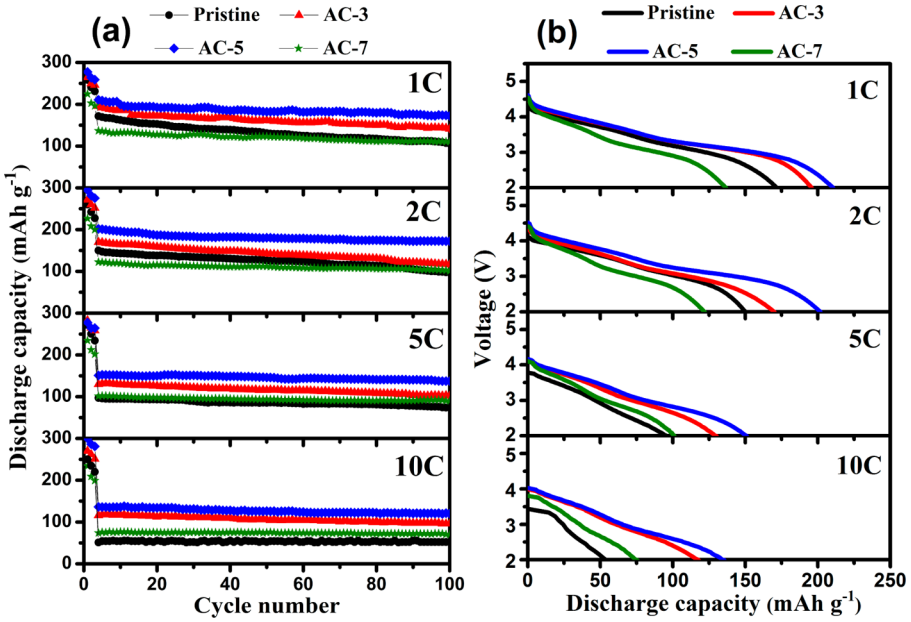

Figure 8. Rate capabilities of all the samples at various high rates (1*C*, 2*C*, 5*C*, and 10*C*): (a) cycling performance; (b) discharge curve at the fourth cycle.

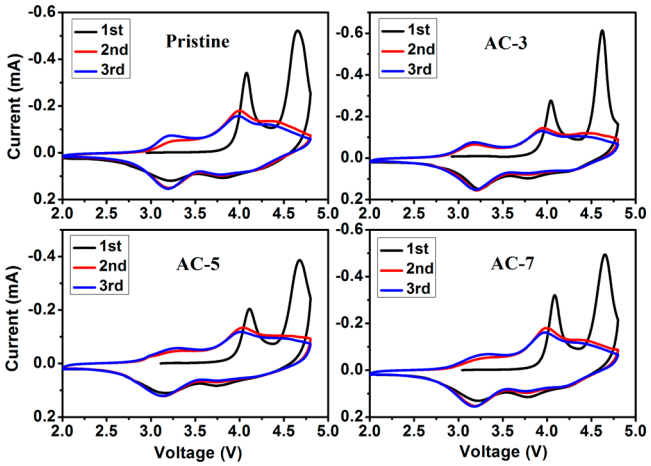

Figure 9. CV curves for three cycles of all the samples.

ohmic resistance (R_Ω), which is almost negligible for both samples. EIS spectra of both samples at charged state of 4 V after 100 cycles at 5*C* are compared. Differently, the semicircle at high frequency stands for the resistance for Li^+ diffusion in the surface layer (R_S) and the semicircle at low frequency reflects the reaction kinetics (R_{ct}). The fitted R_{ct} value of AC-5 after 100 cycles decreases to 65 Ω, lower than that of the pristine sample (220 Ω), demonstrating a much better rate capability. It can be seen that the AC-5 sample exhibits a smaller R_{ct} and R_s than the pristine one, and the lower charge transfer resistance of the AC-5 sample is responsible for its excellent rate capability.

In summary, based on our results in this work, both of the Li_3PO_4 and $AlPO_4$ coating have positive effects on the electrochemical performances of $Li[Li_{0.2}Fe_{0.1}Ni_{0.15}Mn_{0.55}]O_2$ material. $AlPO_4$ phase with the high electronegativity of $(PO_4)^{3-}$ is more beneficial to the cycling stability, whereas as a Li-ion conductor, Li_3PO_4 phase plays a dominant role on the rate performances.

4. CONCLUSION

The layered Li-rich, Fe- and Mn-based cathode material, $Li[Li_{0.2}Fe_{0.1}Ni_{0.15}Mn_{0.55}]O_2$, has been successfully synthesized by a coprecipitation method and further modified with $AlPO_4$. The sample with 5 wt % coating amount shows a significant improvement in discharge capacity, cycling, and rate perform-

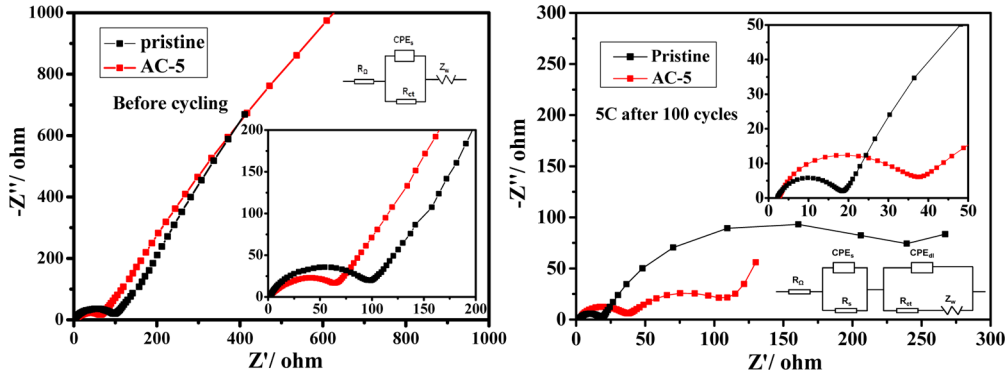

Figure 10. Nyquist plots of the pristine sample and AC-5 before cycling and after 100 cycles at 5*C*.

DOI: 10.1021/am508579r
ACS Appl. Mater. Interfaces 2015, 7, 3773−3781

ances than the pristine one. The excellent electrochemical performances are attributed to the multifunctional $AlPO_4$ surface coating (shown in Scheme 1). A protective layer from the high electronegativity of $(PO_4)^{3-}$ polyanions with Al resists the side reaction between bulk material and the electrolyte and thus enhances the cycling performances. Also, it can retain more oxygen ions vacancies and then leads to a higher discharge capacity. The reduced charge transfer resistance and formation of Li_3PO_4 phase at the surface are responsible for the enhancement in rate capability. This material with both high electrochemical performance and low cost is attractive and gives a new insight for designing and modifying Li-rich cathode materials of the next-generation LIBs.

AUTHOR INFORMATION

Corresponding Authors

*E-mail: lily863@bit.edu.cn.

*E-mail: chenrj@bit.edu.cn.

Author Contributions

F.W., X.Z., and L.L. contributed equally to this work.

Notes

The authors declare no competing financial interest.

ACKNOWLEDGMENTS

The experimental work of this study was supported by the Chinese National 973 Program (2015CB251100), the National Science Foundation of China (NSFC 51302014), Beijing Nova Program (Z121103002512029), and the New Century Educational Talents Plan of the Chinese Education Ministry (NCET-12-0050).

REFERENCES

(1) Armand, M.; Tarascon, J. M. Building Better Batteries. *Nature* **2008**, *451*, 652−657.

(2) Scrosati, B.; Garche, J. Lithium Batteries: Status, Prospects and Future. *J. Power Sources* **2010**, *195*, 2419−2430.

(3) Dunn, B.; Kamath, H.; Tarascon, J. M. Electrical Energy Storage for the Grid: A Battery of Choices. *Science* **2011**, *334*, 928−935.

(4) Goodenough, J. B.; Kim, Y. Challenges for Rechargeable Batteries. *J. Power Sources* **2011**, *196*, 6688−6694.

(5) Yang, Z.; Zhang, J.; Kintner-Meyer, M. C.; Lu, X.; Choi, D.; Lemmon, J. P.; Liu, J. Electrochemical Energy Storage for Green Grid. *Chem. Rev.* **2011**, *111*, 3577−3613.

(6) Melot, B. C.; Tarascon, J. M. Design and Preparation of Materials for Advanced Electrochemical Storage. *Acc. Chem. Res.* **2013**, *46*, 1226−1238.

(7) Thackeray, M. M.; Johnson, C. S.; Vaughey, J. T.; Li, N.; Hackney, S. A. Advances in Manganese-Oxide 'Composite' Electrodes for Lithium-Ion Batteries. *J. Mater. Chem.* **2005**, *15*, 2257−2267.

(8) Thackeray, M. M.; Kang, S. H.; Johnson, C. S.; Vaughey, J. T.; Hackney, S. A. Comments on the Structural Complexity of Lithium-Rich $Li_{1+x}M_{1-x}O_2$ Electrodes (M=Mn, Ni, Co) for Lithium Batteries. *Electrochem. Commun.* **2006**, *8*, 1531−1538.

(9) Thackeray, M. M.; Kang, S.-H.; Johnson, C. S.; Vaughey, J. T.; Benedek, R.; Hackney, S. A. Li_2MnO_3-Stabilized $LiMO_2$ (M = Mn, Ni, Co) Electrodes for Lithium-Ion Batteries. *J. Mater. Chem.* **2007**, *17*, 3112−3125.

(10) Kim, T.-H.; Park, J.-S.; Chang, S. K.; Choi, S.; Ryu, J. H.; Song, H.-K. The Current Move of Lithium Ion Batteries Towards the Next Phase. *Adv. Energy Mater.* **2012**, *2*, 860−872.

(11) Li, J.; Wang, L.; Wang, L.; Luo, J.; Gao, J.; Li, J.; Wang, J.; He, X.; Tian, G.; Fan, S. Synthesis and Characterization of $Li(Li_{0.23}Mn_{0.47}Fe_{0.2}Ni_{0.1})O_2$ Cathode Material for Li-Ion Batteries. *J. Power Sources* **2013**, *244*, 652−657.

(12) Zhao, Y.; Sun, G.; Wu, R. Synthesis of Nanosized Fe-Mn Based Li-Rich Cathode Materials for Lithium-Ion Battery via a Simple Method. *Electrochim. Acta* **2013**, *96*, 291−297.

(13) Armstrong, A. R.; Tee, D. W.; La Mantia, F.; Novák, P.; Bruce, P. G. Synthesis of Tetrahedral $LiFeO_2$ and Its Behavior as a Cathode in Rechargeable Lithium Batteries. *J. Am. Chem. Soc.* **2008**, *130*, 3554−3559.

(14) Tabuchi, M.; Nakashima, A.; Ado, K.; Sakaebe, H.; Kobayashi, H.; Kageyama, H.; Tatsumi, K.; Kobayashi, Y.; Seki, S.; Yamanaka, A. The Effects of Preparation Condition and Dopant on the Electrochemical Property for Fe-Substituted Li_2MnO_3. *J. Power Sources* **2005**, *146*, 287−293.

(15) Tabuchi, M.; Nabeshima, Y.; Takeuchi, T.; Tatsumi, K.; Imaizumi, J.; Nitta, Y. Fe Content Effects on Electrochemical Properties of Fe-Substituted Li_2MnO_3 Positive Electrode Material. *J. Power Sources* **2010**, *195*, 834−844.

(16) Tabuchi, M.; Nabeshima, Y.; Ado, K.; Shikano, M.; Kageyama, H.; Tatsumi, K. Material Design Concept for Fe-Substituted Li_2MnO_3-Based Positive Electrodes. *J. Power Sources* **2007**, *174*, 554−559.

(17) Tabuchi, M.; Shigemura, H.; Ado, K.; Kobayashi, H.; Sakaebe, H.; Kageyama, H.; Kanno, R. Preparation of Lithium Manganese Oxides Containing Iron. *J. Power Sources* **2001**, *97*−*98*, 415−419.

(18) Tabuchi, M.; Nabeshima, Y.; Takeuchi, T.; Kageyama, H.; Tatsumi, K.; Akimoto, J.; Shibuya, H.; Imaizumi, J. Synthesis and Electrochemical Characterization of Fe and Ni Substituted Li_2MnO_3—An Effective Means to Use Fe for Constructing "Co-Free" Li_2MnO_3 Based Positive Electrode Material. *J. Power Sources* **2011**, *196*, 3611−3622.

(19) Sun, Y. K.; Lee, M. J.; Yoon, C. S.; Hassoun, J.; Amine, K.; Scrosati, B. The Role of AlF_3 Coatings in Improving Electrochemical Cycling of Li-Enriched Nickel-Manganese Oxide Electrodes for Li-Ion Batteries. *Adv. Mater.* **2012**, *24*, 1192−1196.

(20) Myung, S.-T.; Izumi, K.; Komaba, S.; Yashiro, H.; Bang, H. J.; Sun, Y.-K.; Kumagai, N. Functionality of Oxide Coating for $Li[Li_{0.05}Ni_{0.4}Co_{0.15}Mn_{0.4}]O_2$ as Positive Electrode Materials for Lithium-Ion Secondary Batteries. *J. Phys. Chem. C* **2007**, *111*, 4061−4067.

(21) Kim, J.; Noh, M.; Cho, J.; Kim, H.; Kim, K.-B. Controlled Nanoparticle Metal Phosphates (Metal = Al, Fe, Ce, and Sr) Coatings on $LiCoO_2$ Cathode Materials. *J. Electrochem. Soc.* **2005**, *152*, A1142−A1148.

(22) Lee, K. T.; Jeong, S.; Cho, J. Roles of Surface Chemistry on Safety and Electrochemistry in Lithium Ion Batteries. *Acc. Chem. Res.* **2012**, *46*, 1161−1170.

(23) Cho, J.; Kim, Y. W.; Kim, B.; Lee, J. G.; Park, B. A Breakthrough in the Safety of Lithium Secondary Batteries by Coating the Cathode Material with $AlPO_4$ Nanoparticles. *Angew., Chem. Int. Ed. Engl.* **2003**, *42*, 1618−1621.

(24) Kim, B.; Lee, J.-G.; Choi, M.; Cho, J.; Park, B. Correlation between Local Strain and Cycle-Life Performance of $AlPO_4$-Coated $LiCoO_2$ Cathodes. *J. Power Sources* **2004**, *126*, 190−192.

(25) Cho, J.; Kim, T.-J.; Kim, J.; Noh, M.; Park, B. Synthesis, Thermal, and Electrochemical Properties of $AlPO_4$-Coated $Li-Ni_{0.8}Co_{0.1}Mn_{0.1}O_2$ Cathode Materials for a Li-Ion Cell. *J. Electrochem. Soc.* **2004**, *151*, A1899−A1904.

(26) Lee, J.-G.; Kim, B.; Cho, J.; Kim, Y.-W.; Park, B. Effect of $AlPO_4$-Nanoparticle Coating Concentration on High-Cutoff-Voltage Electrochemical Performances in $LiCoO_2$. *J. Electrochem. Soc.* **2004**, *151*, A801−A805.

(27) Padhi, A. K.; Nanjundaswamy, K. S.; Goodenough, J. B. Phospho-Olivines as Positive-Electrode Materials for Rechargeable Lithium Batteries. *J. Electrochem. Soc.* **1997**, *144*, 1188−1194.

(28) Appapillai, A. T.; Mansour, A. N.; Cho, J.; Shao-Horn, Y. Microstructure of $LiCoO_2$ with and without "$AlPO_4$" Nanoparticle Coating: Combined STEM and XPS Studies. *Chem. Mater.* **2007**, *19*, 5748−5757.

(29) Lu, Y.-C.; Mansour, A. N.; Yabuuchi, N.; Shao-Horn, Y. Probing the Origin of Enhanced Stability of "$AlPO_4$" Nanoparticle Coated

DOI: 10.1021/am508579r
ACS Appl. Mater. Interfaces 2015, 7, 3773−3781

$LiCoO_2$ during Cycling to High Voltages: Combined XRD and XPS Studies. *Chem. Mater.* **2009**, *21*, 4408−4424.
(30) Wu, Y.; Murugan, A. V.; Manthiram, A. Surface Modification of High Capacity Layered $Li[Li_{0.2}Mn_{0.54}Ni_{0.13}Co_{0.13}]O_2$ Cathodes by $AlPO_4$. *J. Electrochem. Soc.* **2008**, *155*, A635−A641.
(31) Cho, J.; Lee, J. G.; Kim, B.; Park, B. Effect of P_2O_5 and $AlPO_4$ Coating on $LiCoO_2$ Cathode Material. *Chem. Mater.* **2003**, *15*, 3190−3193.
(32) Kim, B.; Kim, C.; Ahn, D.; Moon, T.; Ahn, J.; Park, Y.; Park, B. Nanostructural Effect of $AlPO_4$-Nanoparticle Coating on the Cycle-Life Performance in $LiCoO_2$ Thin Films. *Electrochem. Solid-State Lett.* **2007**, *10*, A32−A35.
(33) Zeng, Y.; He, J. Surface Structure Investigation of $LiNi_{0.8}Co_{0.2}O_2$ by $AlPO_4$ Coating and Using Functional Electrolyte. *J. Power Sources* **2009**, *189*, 519−521.
(34) Liu, D.; He, Z.; Liu, X. Increased Cycling Stability of $AlPO_4$-Coated $LiMn_2O_4$ for Lithium Ion Batteries. *Mater. Lett.* **2007**, *61*, 4703−4706.
(35) Jiao, L.; Liu, L.; Sun, J.; Yang, L.; Zhang, Y.; Yuan, H.; Wang, Y.; Zhou, X. Effect of $AlPO_4$ Nanowire Coating on the Electrochemical Properties of LiV_3O_8 Cathode Material. *J. Phys. Chem. C* **2008**, *112*, 18249−18254.
(36) Rotole, J. A.; Sherwood, P. M. A. Aluminum Phosphate by XPS. *Surf. Sci. Spectra* **1998**, *5*, 60−66.
(37) Shaju, K. M.; Subba Rao, G. V.; Chowdari, B. V. R. Performance of Layered $Li(Ni_{1/3}Co_{1/3}Mn_{1/3})O_2$ as Cathode for Li-Ion Batteries. *Electrochim. Acta* **2002**, *48*, 145−151.
(38) Amine, K.; Tukamoto, H.; Yasuda, H.; Fujita, Y. A New Three-Volt Spinel $Li_{1+x}Mn_{1.5}Ni_{0.5}O_4$ for Secondary Lithium Batteries. *J. Electrochem. Soc.* **1996**, *143*, 1607−1613.
(39) Yamashita, T.; Hayes, P. Analysis of XPS Spectra of Fe^{2+} and Fe^{3+} Ions in Oxide Materials. *Appl. Surf. Sci.* **2008**, *254*, 2441−2449.
(40) Gu, M.; Belharouak, I.; Zheng, J. M.; Wu, H. M.; Xiao, J.; Genc, A.; Amine, K.; Thevuthasan, S.; Baer, D. R.; Zhang, J. G.; Browning, N. D.; Liu, J.; Wang, C. M. Formation of the Spinel Phase in the Layered Composite Cathode Used in Li-Ion Batteries. *ACS Nano* **2013**, *7*, 760−767.
(41) Zhao, S.-X.; Ding, H.; Wang, Y.-C.; Li, B.-H.; Nan, C.-W. Improving Rate Performance of $LiFePO_4$ Cathode Materials by Hybrid Coating of Nano-Li_3PO_4 and Carbon. *J. Alloys Compd.* **2013**, *566*, 206−211.

DOI: 10.1021/am508579r
ACS Appl. Mater. Interfaces 2015, 7, 3773−3781